AMSI VACATION RESEARCH SCHOLARSHIPS 2020–21

Get a Thirst for Research this Summer

Stochastic Modelling of Deterministic Systems

Jack Mulqueeney

Supervised by Dr. Thomas Stemler

The University of Western Australia

Vacation Research Scholarships are funded jointly by the Department of Education, Skills and Employment and the Australian Mathematical Sciences Institute.

Abstract

This paper summarises and applies the Kramers-Moyal expansion and the theory of stochastic resonance to model complex deterministic systems. The Kramers-Moyal expansion is found to accurately model a range of deterministic systems: from a simple stochastic differential equation (SDE) to more complicated electrical circuits. We replicate results from the literature to confirm the method's efficacy and apply it to a novel system, the Lang-Kobayashi Laser equations, and find evidence of interesting dynamical behaviour after a range of numerical simulations. A second method is tested with stochastic resonance to determine the determinstic dynamics of a Lorenz system is properly modelled as noise.

Introduction

Since Einstein's seminal work on Brownian motion in 1905, the field of statistical and stochastic modelling of deterministic systems has grown and applied in many different scientific fields. This paper uses two such methods: the Kramers-Moyal expansion (KME) and a method based on autocorrelation integrals.

The first section of this report is dedicated to the important theoretical underpinnings of our modelling schema. I introduce the Langevin and Fokker-Planck equations, which are the foundation for the KME. The Langevin equation is a SDE with a deterministic component and delta-correlated, Gaussian noise component. Correspondingly, the Fokker-Planck equation, which is an equation of motion for the probability density of a particle, features a drift (deterministic) and diffusion (noise) component. I then present the KME, which integrates and Taylor expands the Langevin equation to estimate the drift and diffusion components of the Fokker-Planck equation, returning an accurate model of the particle's motion.

The second section applies the KME to various systems. We start with a known, basic SDE, allowing me to test and refine my code, ensuring it returns the coefficients accurately. We then investigate the behaviour and residency times in attractor regions for the Chua and Shinriki circuits. The data are distinct, with the Chua being numerically simulated and Shinriki being experimental. We motivate and develop these circuit systems together due to their topological equivalence. I replicate results from Stemler *et al* [1] and confirm the accuracy of our model.

Section three motivates, develops, and applies the method of autocorrelation integrals, that we are going to test with stochastic resonance. The concept behind stochastic resonance is best explained via an example in the biology literature, where the paddlefish optimises successful feeding behaviour in the presence of a non-zero level of environmental interference/noise. We consider these concepts in line with Just [2], who illustrates the concept with a periodically driven double-well potential with noise derived from a Gaussian distribution and a time-scale separated Lorenz system. The model locates the diffusive constant, D, accurately in both cases.

The final section reports on a novel application of the KME to a optically driven laser system modelled by the Lang-Kobayashi rate equations. We find evidence of wildly changing noise profiles under mild changes in the control parameter. My analysis, constrained by available computing power, motivates a further analysis over a wider range of control parameters and in experimental data.

1 Theoretical Foundations

1.1 Non-Linear Langevin Equation

The Langevin equation describes the time-evolution of a particle, separated into slow, $h(x,t)$, and fast,$g(x,t)\Gamma(t)$, degrees of freedom. For one stochastic variable x, the Langevin equation is:

$$\dot{x} = h(x,t) + g(x,t)\Gamma(t) \tag{1}$$

Where $\Gamma(t)$, known as the Langevin force, is assumed to be a Gaussian random variable with zero mean and δ correlation function. We choose the following normalisation of the Langevin force:

$$\begin{aligned} \langle \Gamma(t) \rangle &= 0 \\ \langle \Gamma(t)\Gamma(t') \rangle &= 2\delta(t-t') \end{aligned} \tag{2}$$

1.2 Fokker-Planck Equation

The general Fokker-Planck equation as stated by Risken [3] is:

$$\frac{\partial \rho(x,t)}{\partial t} = \Big[-\frac{\partial}{\partial x} D^{(1)}(x) + \frac{\partial^2}{\partial x^2} D^{(2)}(x) \Big] \rho(x,t) \tag{3}$$

Where $D^{(1)}(x)$ is the drift coefficient and $D^{(2)}(x)$ is the diffusion coefficient. In our context, $\rho(x,t)$ describes the probability distribution of the particle.

1.3 Kramers-Moyal Expansion

A formal solution to equation (1) is usually non-calculable and as such we set up a Fokker-Planck and obtain the following Kramers-Moyal expansion for the n^{th} coefficients

$$D^{(n)}(x,t) = \frac{1}{n!} \lim_{\tau \to 0} \frac{1}{\tau} \langle [x(t+\tau) - x(t)]^n \rangle \tag{4}$$

To derive the above, we first obtain the equivalent integral equation of the stochastic differential equation presented in equation (1)

$$x(t+\tau) - x(t) = \int_t^{t+\tau} [h(x(t'),t') + g(x(t'),t')\Gamma(t')] \mathrm{d}t' \tag{5}$$

Let us assume that h and g can be expanded as follows:

$$\begin{aligned} h(x(t'),t') &= h(x(t),t') + h'(x(t),t')(x(t') - x(t)) + \dots \\ g(x(t'),t') &= g(x(t),t') + g'(x(t),t')(x(t') - x(t)) + \dots \end{aligned} \tag{6}$$

Where h' and g' are the $x = x(t)$ derivatives of h and g, respectively. Substituting the Taylor's expansion of equation (5) into equation (4) yields:

$$\begin{aligned} x(t+\tau) - x(t) = &\int_t^{t+\tau} h(x(t),t')\mathrm{d}t' + \int_t^{t+\tau} h'(x(t),t')(x(t') - x(t))\mathrm{d}t' + ... \\ &+ \int_t^{t+\tau} g(x(t),t')\Gamma(t')\mathrm{d}t' + \int_t^{t+\tau} g'(x(t),t')(x(t') - x(t))\Gamma(t')\mathrm{d}t' + ... \end{aligned} \tag{7}$$

We iterate equation (6) into itself which yields:

$$\begin{aligned} x(t+\tau) - x(t) = &\int_t^{t+\tau} h(x(t),t')\mathrm{d}t' + \int_t^{t+\tau} h'(x(t),t') \int_t^{t'} h(x(t),t'')\mathrm{d}t''\mathrm{d}t' \\ &+ \int_t^{t+\tau} h'(x(t),t') \int_t^{t'} g(x(t),t'')\Gamma(t'')\mathrm{d}t''\mathrm{d}t' + ... \\ &+ \int_t^{t+\tau} g(x(t),t')\Gamma(t')\mathrm{d}t' + \int_t^{t+\tau} g'(x(t),t') \int_t^{t'} h(x(t),t'')\Gamma(t')\mathrm{d}t''\mathrm{d}t' \\ &+ \int_t^{t+\tau} g'(x(t),t') \int_t^{t'} g(x,t'')\Gamma(t'')\Gamma(t')\mathrm{d}t''\mathrm{d}t' + ... \end{aligned} \tag{8}$$

By repeating the substitution, we get a right-hand side that only depends on Langevin force $\Gamma(t)$, the known functions $g(x,t)$, $h(x,t)$, and their derivatives. By taking averages and by making use of the assumption detailed in equation (2) about $\Gamma(t)$ we have:

$$\begin{aligned} \langle x(t+\tau) - x(t)\rangle = &\int_t^{t+\tau} h(x(t),t')\mathrm{d}t' + \int_t^{t+\tau} \int_t^{t'} h'(x(t),t')h(x(t),t'')\mathrm{d}t''\mathrm{d}t' + ... \\ &+ \int_t^{t+\tau} g'(x(t),t') \int_t^{t'} g(x(t),t'')2\delta(t'' - t')\mathrm{d}t''\mathrm{d}t' + ... \end{aligned} \tag{9}$$

By the choice of a symmetric density δ around the origin, we achieve the following equality:

$$\int_t^{t'} g(x(t),t'')2\delta(t'' - t')\mathrm{d}t''\mathrm{d}t' = g(x(t),t') \int_t^{t'} 2\delta(t'' - t')\mathrm{d}t'' = g(x(t),t') \tag{10}$$

And thus by taking $\tau \to 0$ and substituting equation (10) into equation (9) we derive:

$$D^{(1)}(x(t),t) = h(x(t),t) + \frac{\partial g(x(t),t)}{\partial x(t)} g(x(t),t) \tag{11}$$

A symmetric argument applies when deriving the form of $D^{(1)}(x(t),t)$, the diffusion coefficient

$$\begin{aligned} D^{(2)}(x(t),t) &= \frac{1}{2} \lim_{\tau \to 0} \frac{1}{\tau} \int_t^{t+\tau} \int_t^{t+\tau} g(x(t),t')g(x(t),t'')2\delta(t' - t'')\mathrm{d}t'\mathrm{d}t'' \\ &= g^2(x(t),t) \end{aligned} \tag{12}$$

Applying such a method to time series environments, we have the following

$$\begin{aligned} \delta t D^{(1)}(X) &= \langle [x(t+\delta t) - x(t)]\rangle + o(\delta t) = h(x(t),t) + \frac{\partial g(x(t),t)}{\partial x(t)} g(x(t),t) \\ 2\delta t D^{(2)}(X) &= \langle [x(t+\delta t) - x(t)]^2\rangle + o(\delta t) = g^2(x(t),t) \end{aligned} \tag{13}$$

Encouragingly, the expansion returns the deterministic and noise functions (h and g) of the non-linear Langevin equation in equation (1).

2 Modelling via Kramers-Moyal

2.1 The Basic SDE

As a first check on the Kramers-Moyal expansion, I first model a basic stochastic differential equation defined as:

$$\dot{x} = f(x) + \sqrt{D}\Gamma \tag{14}$$

Where $f(x)$ is the deterministic drift component and $\sqrt{D}\Gamma$ is the noise component, where $\sqrt{D}$ is the diffusion coefficient. Firstly, we need to simulate a time series of this system. To do this, we consider an Euler expansion of the system

$$\dot{x} \approx x(t + \Delta t) = x(t) + \Delta x = x(t) + f(x)\Delta t + \sqrt{D}\Delta W \tag{15}$$

Where $x(t)$ is the time series realisation at time t, Δt is a time increment, $f(x)$ and $\sqrt{D}$ are as above, and $\Delta W = (\phi' - \phi)\sqrt{\Delta t}$ is the standard Wiener increment where x' and x are independent realisations of a Gaussian white noise process. A realisation is presented below for $D = 0.2$ and $f(x) = x - x^3$.

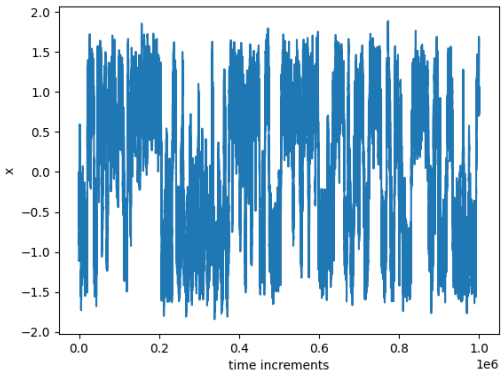

Figure 1: Time series generated via Euler expansion of eq. (13)

After generating the time series, we can calculate the drift and diffusion coefficients by considering small horizontal bins of the time series, calculating the coefficient, and taking the mean of all the coefficient realisations. As shown in Figure 2, the generation of the drift and diffusion coefficients is accurate and reflects the chosen values in the system, which is encouraging in applying the method on increasingly complex systems.

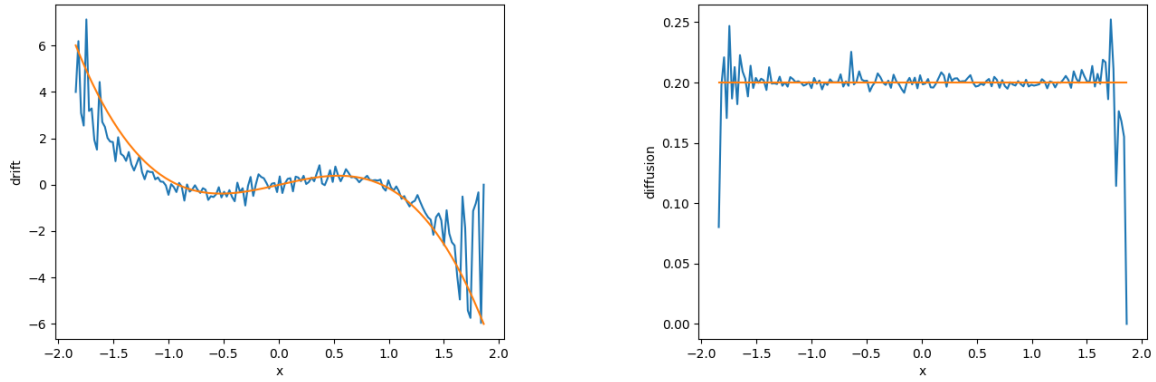

(a) Drift

(b) Diffusion

Figure 2: Drift and Diffusion from simulated time series of eq. (13)

2.2 Electrical Circuit Investigations

We now turn to two electrical circuit systems, the Chua and Shinriki. The Chua system is governed by the dynamical system:

$$\dot{x} = \alpha\big[y - x - f(x)\big], \tag{16}$$

$$RC_2\dot{y} = x - y + Rz, \tag{17}$$

$$\dot{z} = -\beta y \tag{18}$$

2.2.1 Chua Data

We generate data from the above system from Python. This analysis will focus exclusively on the time series generated in the x-coordinate, shown below. The above dynamical system exhibits chaos and a well-known double attractor, known as the "double-scroll", which is the focus of our analysis. We particularly model the 'jumping' or transitions from one attractor to another, which we will dub the slow degrees of freedom. These dynamics correspond to the sudden attractor widening crisis, described in the bifurcation diagram at around $\alpha = 9.14$ and shown in the pre-critical and post-critical comparison diagrams. The parameters used are $\beta = -15$, $RC_2 = 1$, and $R = 1$.

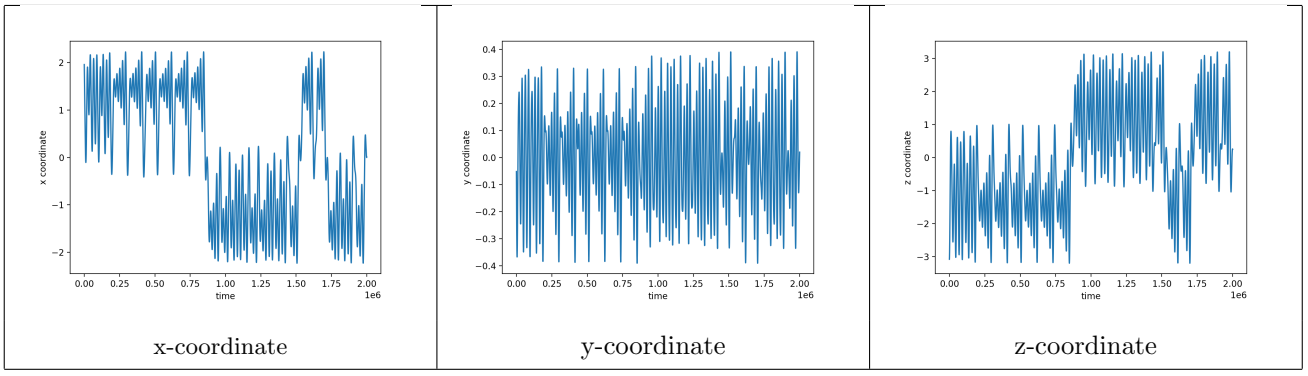

x-coordinate | y-coordinate | z-coordinate

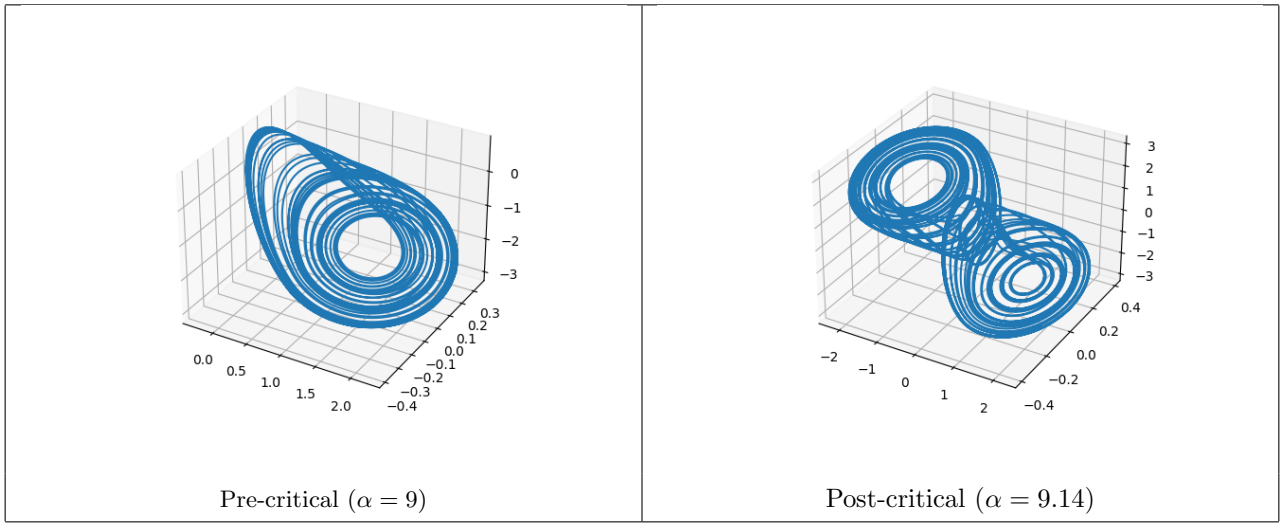

Pre-critical ($\alpha = 9$) | Post-critical ($\alpha = 9.14$)

2.2.2 Shinriki Circuit/Data

An extended discussion of the Shinriki experimental setup is available in Stemler et al [1]. To summarise for completeness, the setup consists of an RLC circuit coupled to an RC element via two Zener diodes $Z_{1,2}$, producing a nonlinearity in the measurements.

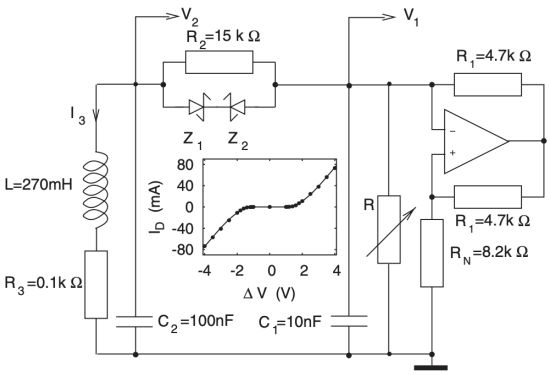

Figure 3: Shinriki oscillator setup as in [1], with nonlinearity of the Zener diodes in the inset graph.

This nonlinearity is exhibited in the inset of Figure 3, obtained from Stemler *et al* [1]. The control parameter is encapsulated in the resistor R, which controls the current supplied to the oscillatory components of the circuit. The circuit exhibits the standard period-doubling route to chaos via increasing the control parameter R, and the desired intermittency is exhibited after $R_c = 66\text{k}\Omega$. Intermittent switching between attractors arises in this system in a classical way as first discussed by Grebogi *et al* [4]. When $R < R_c = 66\text{k}\Omega$, two attractors with corresponding basins of attraction, and separated by a boundary, simultaneously touch the boundary and the attractors

enlarge, or "merge". For a small perturbation above R_c, the system exists in one attractor region for an extended period, and abruptly transitions to the other attractor region. This switching we refer to the slow degrees of freedom. The time scale of the slow degrees of freedom adheres to a rather simple law $\tau \approx |R - R_c|^{-\gamma}$ [4]. These slow dynamics are contrasted to the fast dynamics in the transitions between states within pre-critical attractor regions. The aim of the our constructed stochastic model is to recreate the intermittent behaviour of the system.

2.2.3 Analysis

As in the simple stochastic differential equation in section 2.1, we build up the drift and diffusion coefficients. However, firstly we must plot how these coefficients vary as a function of the size of the lag. This ensures a suitable level of chaotic mixing such that the necessary high autocorrelations for low time lags decay to a point resembling a random process. We justify this process by appealing to the positive entropy of chaotic attractors. Autocorrelations for low lags are greater, and as such information in the attractor is greater. As the lag increases, the autocorrelations and information decay as a result from the positive entropy. Before the square root decay most evident in the Shinriki lag dependency plot, a plateau arises which corresponds to the transition from a relatively high information correlation regime to one resembling a random process. In this plateau can we maintain a degree of information regarding the dynamics while maintaining the suitability of stochastic model. The resultant plots for each circuit are below.

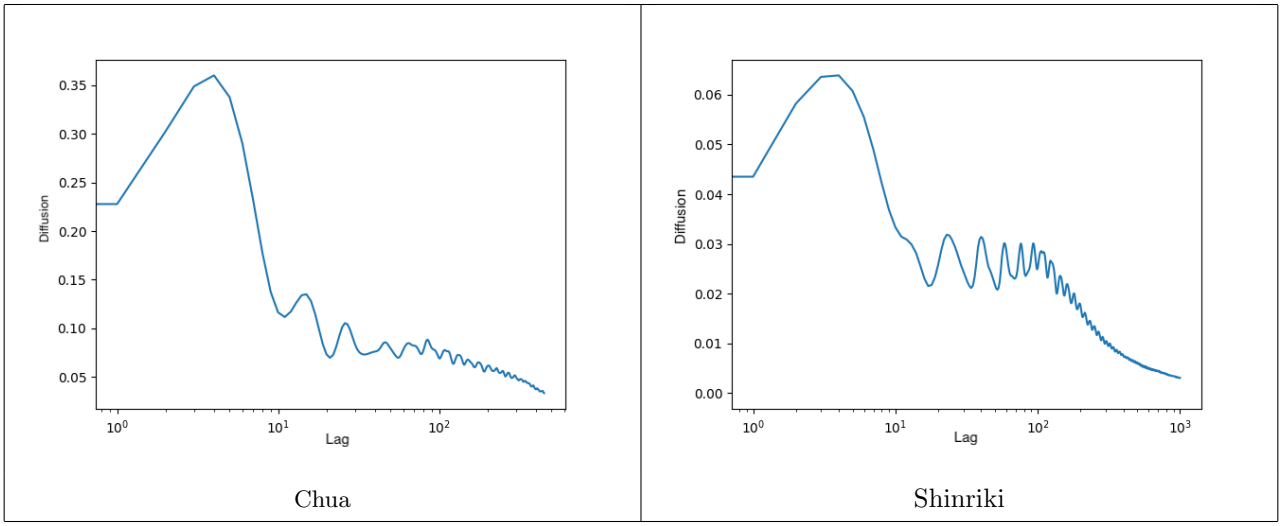

Chua | Shinriki

Plateaus emerge for $40 < \tau < 80$ and $20 < \tau < 100$ for the Chua and Shinriki circuits, respectively. This lag allows to construct a model for the transitions between attractor wings in the post-critical dynamical regime for the $x-$coordinate. We will compare actual residence times with calculated residence times in attractor wings with those predicted by the Fokker-Planck equations.

It is in these ranges of values that we select a lag to construct plots of the drift and diffusion for the Shinriki circuit. In the computation, we select a range of lags in the plateau region corresponding to two oscillations

of lag dependency of $D^{(2)}$. The drift and diffusion plots for control parameter $\Delta R = 1.15\text{k}\Omega$ demonstrating a linear decay. Although it is not needed for the remaining analysis, the analogous plot for diffusion coefficients is shown. $D^{(2)}$ is an inverted parabola. If we let α be the gradient of the decay of $D^{(1)}$, and the inverted parabola $D^{(2)} = D(z_0^2 - z^2)$, we obtain the following Fokker-Planck equation

$$\frac{\partial \rho(z,t)}{\partial t} = \alpha \frac{\partial \rho(z,t)}{\partial z} + D \frac{\partial^2 \rho(z,t)(z_0^2 - z^2)}{\partial t^2} \tag{19}$$

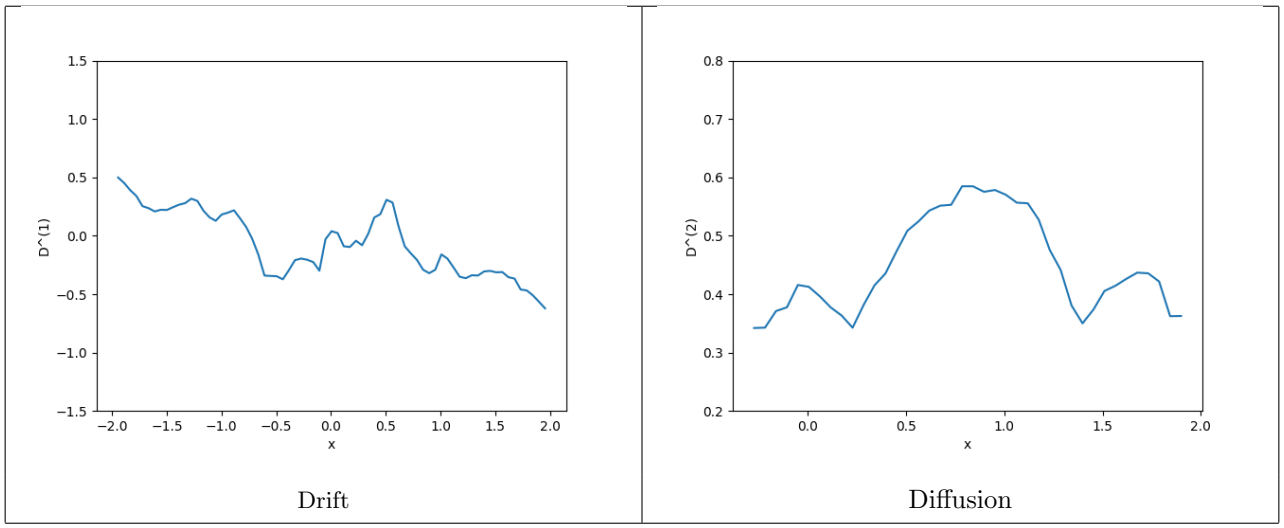

Drift Diffusion

From Stemler *et al* [1], the eigenvalues of the Fokker-Planck operator, governing the time evolution of the system, are given by $\Lambda_n = -n\alpha - n(n-1)D$, which yields slow jumping following the equation $\tau = 2/|\alpha|$. Calculating α over a continuum of control parameters $10.7\text{k}\Omega \leq R_c \leq 19.9\text{k}\Omega$ then allows us to predict the mean occupation times in each attractor. Comparing such predictions to the observed occupation times given by the data yields Figure 4. The close resemblance between the observed (blue) and predicted occupation times (orange) is evidence that the developed stochastic model effectively captures the slow jumping dynamics evident in the Shinriki oscillator. Deviations with lower critical can be explained by the very fact of longer residency times. Access to the necessary number of attractor jumps to generate suitable statistics for the analysis decays when residency times are longer, hence the deviations. The sudden negative spike in residency times around $R_c = 1.6\text{k}\Omega$ corresponds to the emergence of a periodic window, which necessarily decreases residency times during its existence.

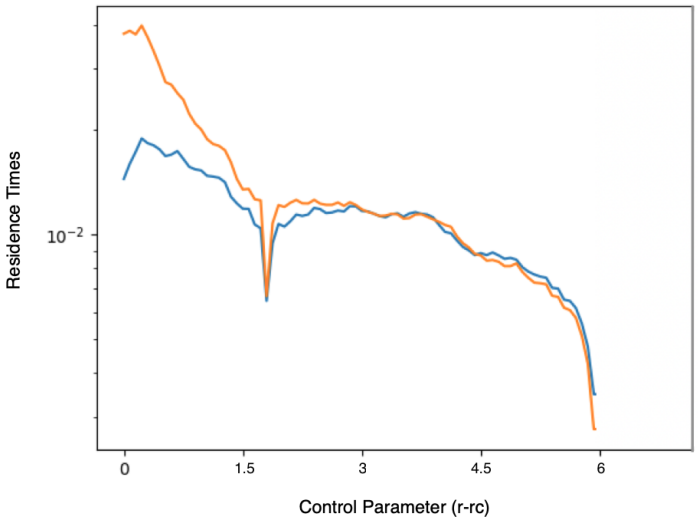

Figure 4: Occupation times vs. critical parameter

3 Stochastic Resonance

3.1 Background and Motivating Example

Stochastic resonance, as described by McNamara and Wiesenfeld [5], is the maximisation of some measure of signal "clarity" given an input of a non-zero noise level. Consider a bistable physical system such as a double-well potential. By adding a random forcing component, such as a periodic driver $a\cos(\omega t)$, where ω is the frequency of the driver, the system will oscillate near the two stable points of the wells, but transition occasionally across the barrier between the wells. Increasing the noise variance, D, increases the probability of these jumps and hence the rate at which the particle transitions between the wells. Graphically speaking, the periodic driver modulates the wells slightly, increasing the probability of being in one well over the other. Letting $W_+(t)$ be the jump rate from the $+$ well and $W_-(t)$ be the jump rate from the $-$ well, the jump rate between wells is simply $\alpha = W_+(t) + W_-(t)$. Given the periodicity of the driver, $W_+(t)$ being maximised implies that $W_-(t)$ maximises half a period later $-$ giving characteristic jumps two and from attractors discussed in the previous section.

Using the vocabulary of signals, we consider the position of the particle $x(t)$ as the output and focus on the power spectrum $S(\Omega) = |X(\Omega)|^2$ of $x(t)$, where $X(\Omega)$ is the Fourier transform of $x(t)$. Given the power spectrum, we find that the output noise power increases until $\alpha \approx \omega_s$, where ω_s is the signal frequency. This is the idea behind stochastic resonance $-$ increasing D increases α (until a point), eventually maximising the output noise power.

The theory behind stochastic resonance is perhaps best illustrated by an example from the evolutionary biological literature by Freund *et al* [6] involving a paddlefish foraging for the zooplankton Daphnia. Freund *et al* found that noise plays an important role in optimising foraging search strategies. Inhabiting muddy waters, the paddlefish use electroreceptor organs distributed over their rostrum (their nose; the paddle) which

helps detect the Daphnia without relying on normal vision [6]. The Daphnia power spectrum is dipolar at 7Hz (the feeding frequency of interest) and 14Hz (iron and other minerals convection currents within singular Daphnia). Importantly, noise is added to the system as a result of the movement of individual Daphnia and their swarming behaviour: Oscillatory signals from single organisms are incoherent from one another, and their frequency vectors point in all directions and are uncorrelated; thus, the frequency emitted by the swarm will be perceived by the paddlefish as Gaussian white noise by the Central Limit Theorem. And so a single Daphnia swimming outside of the swarm can be detected by the paddlefish by means of stochastic resonance. A single Daphnia swimming outside the swarm provides the "subthreshold" frequency observed by the paddlefish, the "threshold" frequency stemming from the properties of the electroreceptive organs in the rostrum, and noise by virtue of the uncorrelated aggregation of movements in Daphnia swarms. The essence of stochastic resonance is that the paddlefish performs better in terms of its feeding behaviour in the presence of a certain degree of noise, their prey's proximity to a swarm.

3.2 Simulations and Modelling

As a simple example, we simulate and study the dynamics of a particle in a periodically-driven double well potential with a Lorenz component, as in Just *et al* [2]:

$$\begin{aligned} \dot{x} &= x - x^3 + a\cos(\omega t) + \kappa y_1 \\ \dot{y}_1 &= \frac{\sigma}{\varepsilon}(y_2 - y_1) \\ \dot{y}_2 &= \frac{1}{\varepsilon}(r y_1 - y_1 y_3 - y_2) \\ \dot{y}_3 &= \frac{1}{\varepsilon}(y_1 y_2 - b y_3) \end{aligned} \tag{20}$$

The y_1 component of the Lorenz system above plays the role of random noise being fed into the periodically driven double well potential. We contrast the above deterministic noise with simply feeding Gaussian random noise with strength given by diffusion constant D, as in 2.1. By fixing ε and adjusting κ, we in effect increase the separation between components and the strength of the deterministic noise. Hence, we can calculate an effective diffusion constant, D, for systems with the deterministic noise component κy_1

$$D = \varepsilon\kappa^2 \int_0^\infty \langle y_1(t') y_1(t'+t) \rangle_{t'} dt \tag{21}$$

For $\kappa > 0$ and hence $D > 0$, the particle has non-zero probability of jumping from one well to another, approximated by the well-known Kramer's rate $1/T_K = \exp(-\Delta/D)$, where $\Delta = 1/4$ is the height of the barrier and D is defined as above. Maximal synchronisation between jumps and periodic driving occurs when $2\pi/\omega = 2T_K$. We use the correlation index, c,

$$c = \sqrt{\langle x(t)\cos(\omega t)\rangle_t^2 + \langle x(t)\sin(\omega t)\rangle_t^2} \quad [2] \tag{22}$$

to compute the signal "clarity" and demonstrate that a non-zero level of noise maximises the correlation between the driving and the state of the system over time.

Firstly, we model stochastic resonance simply with stochastic additive noise as in subsection 2.1, and compare this with noise derived from the Lorenz system with time-scale separation defined by $\varepsilon << 1$. In line with Just *et al* [2], we choose $\varepsilon = 0.005$. Clearly, the system exhibits stochastic resonance as we go through an effective diffusion constant, $\sqrt{D}$ of $0.2 - 0.3$. Comparing this to the system

$$\dot{x} = x - x^3 + a\cos(\omega t) + \sqrt{D}\Gamma \tag{23}$$

Where Γ is Gaussian white noise, we see similar shapes for the stochastic resonance curve going through $0.2 \leq \sqrt{D} \leq 0.3$.

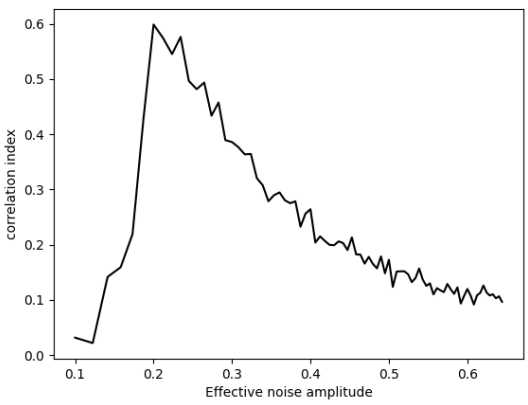

Stochastic resonance from noise (Equation 23)

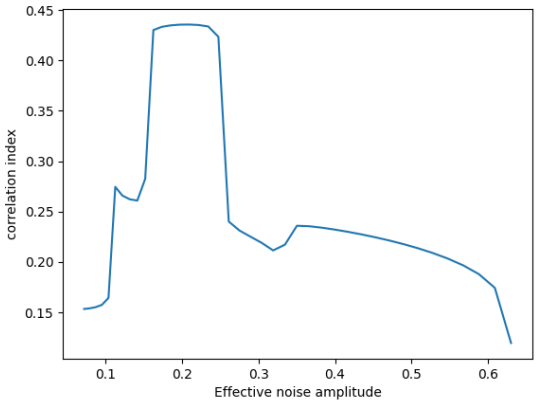

Stochastic resonance from Lorenz y_1 (Equation 20)

4 Optically Driven Laser

The motivation for the following analysis stems from Oliver *et al* [7], who analysed the consistency properties of optically driven laser system.

4.1 System and Lang-Kobayashi Rate Equations

The physical system is rather simple and corresponds to our data generating algorithm. The semiconductor laser is to a short and long optical fibre wire. One of these loops are inputted back into the laser. As a model for our laser, we select the Lang-Kobayashi rate equations as in Oliver *et al* [7]. Their full equations read:

$$\dot{E} = \frac{1+i\alpha}{2} G_N n E + \kappa E_\tau \tag{24}$$

$$\dot{n} = (p-1)\gamma N_{sol} - (\Gamma + G_N n)|E|^2 \tag{25}$$

with the parameters $G_N = 2.142 \times 10^{-5} ns^{-1}$, $\Gamma = 357 ns^{-1}$, $\gamma = 0.909 ns^{-1}$, $N_{sol} = 170.7M$. The pump current is defined by $p = I/I_{th}$. The Poincare-Bendixson theorem states that chaotic dynamics can only arise in three or more dimensions. This may at the outset pose a problem for the Lang-Kobayashi equations above, however the inclusion of the E_τ (a τ-lagged electric field) guarantees as a quasi-infinite dimensional system. E corresponds to the electric field of our laser and n the population of excited electrons.

The following analysis will simulate these equations and compare the developed stochastic analysis derived from a Kramers-Moyal expansion of the Fokker-Planck equation defining transitions between attractors. Firstly, we must generate a long-enough time series of the above system.

4.2 Time Series Overview

Considering the complex valued coordinate E, we cannot use raw simulated data for the KME. Rather, we focus on a synchronisation generation process. Essentially, this requires looking at two different systems for E

$$\dot{\mathbf{x}}_1(t) = \mathbf{f}(\mathbf{x}_1(t)) + \kappa \mathbf{k}(\mathbf{x}_1(t-\tau))$$
$$\dot{\mathbf{x}}_2(t) = \mathbf{f}(\mathbf{x}_2(t)) + \kappa \mathbf{k}(\mathbf{x}_1(t-\tau)) + \text{Noise}$$

The two systems correspond to an unperturbed, 'pure' system, while the other delay system is perturbed with our standard $\sqrt{D}\Gamma$ noise process. Notice that both systems are delayed on the pure system, $\mathbf{x}_1$. This corresponds to the physical setup of two delayed loops, and as such we vary the delay length for each system. We simulate the above for 1.5×10^9. Undefined parameters are defined as: $D = 0.3, \kappa = 0.3, \alpha = 10, p = 20$. As expected, we cannot use the raw simulation data to Importantly, the following analyses deviate from previous systems in the fundamental structure of the dynamics. The first difference is we are no longer modelling an attractor widening crisis with intermittent jumping between attractor wings. Rather, the generated time series more resembles a "firing" process, in which the system sporadically jumps, or "fires" and then resolves back to near the origin.

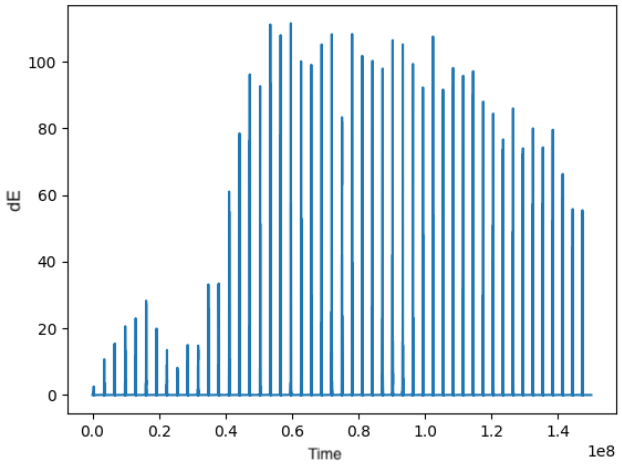

Figure 5: ΔE_t ($\tau_1 = 50$, $\tau_2 = 52$)

The second difference is insufficient time-scale separation. The system is rather slow, and hence we cannot easily generate enough "firings" to guarantee sufficient statistics for both KME and stochastic resonance. So, we manipulate the data to generate further firings by comparing the difference between $\text{Re}(E_{t,\tau_1})$ and $\text{Re}(E_{t,\tau_2})$ where $\tau_2 > \tau_1$. The data of interest is rather $\Delta E_t = \Big(\text{Re}(E_{t,\tau_1}) - \text{Re}(E_{t,\tau_2})\Big)^2$. Applying the above process increase the number of firings by approximately 3 times, which is now sufficient for the statistical analyses applied above.

4.3 Analysis

4.3.1 Kramers-Moyal Expansion

We first attempt to estimate the coefficients to the Fokker-Planck equation governing transitions between attractors present in the Lang-Kobayashi rate equations. We implement an analogous analysis methodology as presented and implemented at length above. We now must generate time series for control parameters $p_1 = 2.5$ and $p_2 = 5$ for $\tau_1 = 50$ and $\tau_2 = 52$.

First, we plot $D^{(2)}$ against choices of lag. Here, we identify a plateau in the region $200 \leq \delta t \leq 400$. The diffusive plateau is of theoretical and computational interest. Integrating and averaging over this region ensures a suitable level of chaotic mixing such that our stochastic modelling regime, with delta correlated noise, is suitable for the non-delta correlated deterministic process. This allows us to average our diffusion computations over a range of lags, granting better statistics and hence more accurate results. After integrating over these lags for both p_1 and p_2, we can inspect the shape of $D^{(2)}$ at each of these parameters, paying particular attention to how it changes depending on p. For both choices of control parameter, we see an upward sloping quadratic, which changes from different control parameters. The positive quadratic shape implies a slightly different form for the potential Fokker-Planck equation describing the density of the system. Despite these rather promising results for a KME of the Lang-Kobayashi equations, the accuracy of such a model remains to be verified and my doing so is constrained by available computing power.

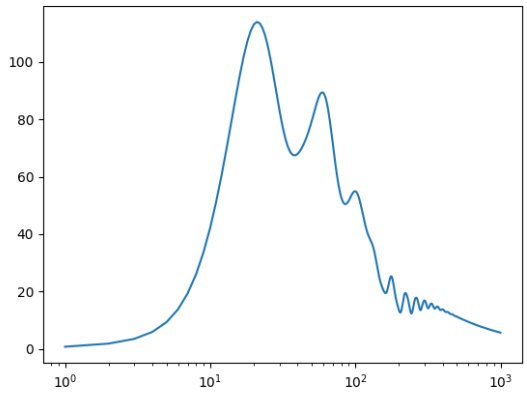

Figure 6: ΔE_t ($p_1 = 2.5, \tau_1 = 50$, $\tau_2 = 52$)

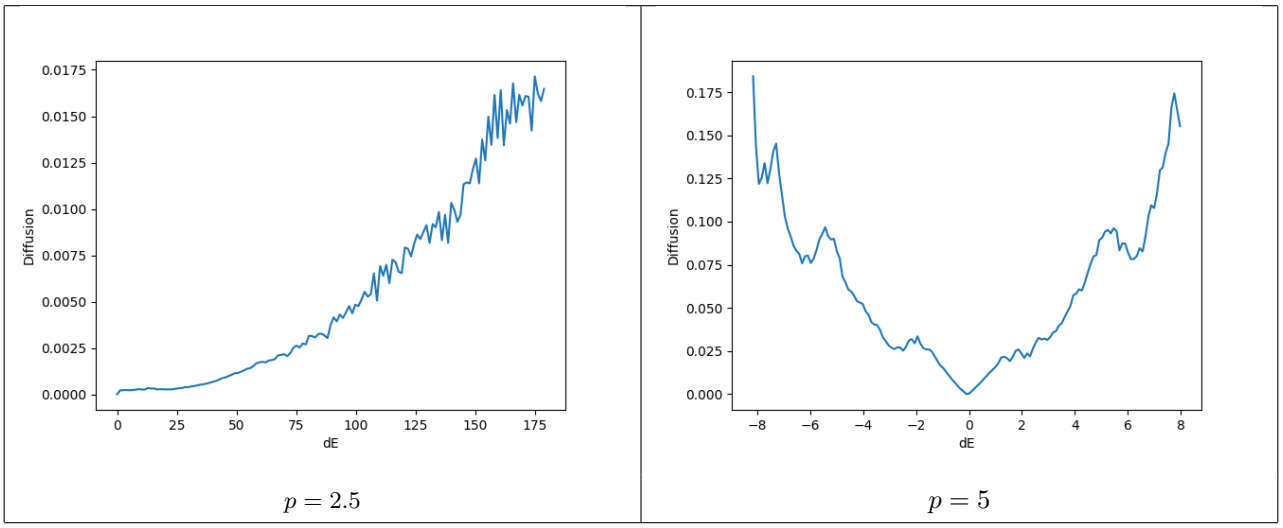

$p = 2.5$ $p = 5$

The drastically changing noise profiles is worth discussing. For $p = 2.5$, we see a weak noise process near the ground state and increasing amplitude in higher states. This is contrasted to the symmetric noise profile for $p = 5$, where extreme positions feature extreme noise, while median regions experience lower noise.

Unfortunately, the analysis could not be completed due to the length of necessary time series for adequate statistical analysis. Further research would further investigate the system at different values of the control parameter. Such an analysis may provide the motivation to examine the experimental data and potentially generate novel insights into the system in terms of modelling its dynamics.

Conclusion

The KME proves effective at modelling deterministic systems. We have shown its applicability for a range of systems, both numerically generated and experimental data. Indeed, its reproduction of the necessary deterministic and noise components to model systems with sufficient time scale separation. Furthermore, we investigated stochastic resonance as another regime to calculate effective noise amplitudes in deterministic systems. Using the KME, we find evidence of drastic deviations in noise profiles for the Lang-Kobayashi equations as a model for an optically driven semiconductor laser.

Further avenues of research would expand our analysis of the Lang-Kobayashi equations for a greater range of differing control parameters to fully grasp the noise profile dynamics. Further, numerically generated data must be used to evaluate the efficacy of the KME in motivating the relevant Fokker-Planck equation to found a similar residency time analysis as outlined in the report. Evidence of effective residency time models would then provide an encouraging foundation to base a similar analysis of experimental data of the optically driven semi-conductor system. Further research would also consider stochastic resonance as a possible avenue for determining effective noise amplitudes in the laser system.

Acknowledgements

I would like to acknowledge and thank my supervisor Dr. Thomas Stemler for his insight and advice regarding both the theoretical and computational components of this project. From poring over lines of Python, to pointing out typos, and giving presentation advice, Dr. Stemler was invaluable to my sanity and completion of the project. I want to thank AMSI for the opportunity and funding to conduct my project.

References

[1] T Stemler, J. Werner, H. Benner, and W. Just, "Stochastic modelling of experimental chaotic time series," *Phys. Rev. Lett.*, vol. 98, 2007.

[2] W Just, H Kantz, C Rodenback, and M. Helm, "Stochastic modelling: Replacing fast degrees of freedom by noise," *J. Phys. A: Math. Gen.*, vol. 34, 2000.

[3] H Risken, *Fokker-Planck Equation: Methods of Solutions and Application*. 1989.

[4] C Grebogi, E Ott, P Romeiras, and J. Yorke, "Critical exponents for crisis-induced intermittency," *Phys. Rev. Lett.*, vol. 36, 1987.

[5] B McNamara and K. Wiesenfeld, "Theory of stochastic resonance," *Phys. Rev. Lett.*, vol. 39, 1989.

[6] J. Freund, L. Schimansky-Geier, B. Beatrix, A. Neiman, D. Russel, T. Yakusheva, and F. Moss, "Behavioral stochastic resonance: How the noise from a daphnia swarm enhances individual prey capture by juvenile paddlefish," *Journal of Theoretical Biology*, vol. 214, 2002.

[7] N. Oliver, T. Jungling, and I. Fischer, "Consistency properties of a chaotic semiconductor laser driven by optical feedback," *Phys. Rev. Lett.*, vol. 114, 2015.